



HAL
open science

Topological protection of electronic states against disorder probed by their magnetic moment

Athmane Tadjine, Christophe Delerue

► **To cite this version:**

Athmane Tadjine, Christophe Delerue. Topological protection of electronic states against disorder probed by their magnetic moment. *Physical Review B*, 2017, 95 (23), pp.235426. 10.1103/PhysRevB.95.235426 . hal-02906814

HAL Id: hal-02906814

<https://hal.science/hal-02906814>

Submitted on 31 May 2022

HAL is a multi-disciplinary open access archive for the deposit and dissemination of scientific research documents, whether they are published or not. The documents may come from teaching and research institutions in France or abroad, or from public or private research centers.

L'archive ouverte pluridisciplinaire **HAL**, est destinée au dépôt et à la diffusion de documents scientifiques de niveau recherche, publiés ou non, émanant des établissements d'enseignement et de recherche français ou étrangers, des laboratoires publics ou privés.

Topological protection of electronic states against disorder probed by their magnetic moment

Athmane Tadjine and Christophe Delerue*

Université Lille, CNRS, Centrale Lille, ISEN, Université Valenciennes, UMR 8520-IEMN, F-59000 Lille, France

(Received 25 April 2017; published 20 June 2017)

Magnetic moments (MMs) of electrons in topological insulator quantum dots (TI-QDs) are investigated using a model system, namely a multiorbital honeycomb lattice. Their nature and orientation with respect to the spin are studied. We show that large MMs are not specific to edge states in nontrivial gaps, as band states can host even larger MMs. However, we demonstrate that edge-state and band-state MMs have a totally different sensitivity to disorder. Measuring the MMs in TI-QDs is therefore a direct way to probe the nontrivial to trivial topological transition under increasing disorder.

DOI: [10.1103/PhysRevB.95.235426](https://doi.org/10.1103/PhysRevB.95.235426)

Since the discovery of topological insulators (TIs) [1–6], topology has pervaded all domains of physics, including ultracold atomic gases [7–9], polariton artificial lattices [10–12], acoustic systems [13,14], and mechanical lattices [15,16]. Among TIs [17–22], two-dimensional (2D) materials characterized by a Z_2 topologically invariant $\nu = 1$ under time-reversal symmetry [23–25] exhibit helical edge states in their band gap. These states are of high interest for spintronics and for the realization of topological quantum states that exhibit non-Abelian statistics [26–28].

In contrast to band states (in the bulk energy bands), these edge states (in the gaps) are characterized by a spin-propagation–direction locking and a topological protection against disorder. However, the different behavior of edge and band states under the effect of disorder is not trivial to reveal and to compare experimentally.

In this paper, we show that measurement of magnetic moments (MMs) in quantum dots of 2D TIs (TI-QDs) provides direct insight into the resistance of the states to disorder, enabling a clear distinction between band and edge states. Large MMs were recently predicted for edge states in TI-QDs [29,30]. Due to time-reversal symmetry, these states form doublets of opposite MMs. The MM of each state could be measured by applying an external magnetic field and by placing the Fermi energy between the split states using electrostatic gating. However, a large MM is not a signature of an edge state in a topological gap. It was already shown that, in a TI-QD of a Bi(111) bilayer [30], large MMs also appear in band states. We show in the following that the case of Bi TI-QDs is not specific, and therefore band and edge states cannot be distinguished by the intensity of their MM. However, we demonstrate that band- and edge-state MMs have drastically different sensitivity to disorder.

In the following, we present calculations of electronic states and MMs in TI-QDs built from a prototypical multiorbital TI characterized by several nontrivial gaps induced by spin-orbit coupling (SOC). We show that the MM of band states can be large, in our example up to twice as large as for edge states. In contrast with edge states, the orientation of a band-state MM is not correlated to the direction of the spin. We also explain the origin of the MMs in terms of spin-orbit-induced

circulating currents (SOICCs). Band states and their associated SOICCs are not topologically protected against disorder. Therefore, under moderate disorder, their MMs are strongly suppressed while edge-state MMs are almost unaffected. At strong disorder, all MMs collapse. This provides a window in terms of disorder where edge states can be clearly identified from band states.

We consider electrons on a honeycomb lattice with one s and three p orbitals per site. Including the spin degree of freedom, this results in a 16-band model. The effective Hamiltonian is written quite generally as [2,31,32]

$$\begin{aligned} & \sum_i \sum_{\alpha, \beta} E_b c_{i, \beta, \alpha}^\dagger c_{i, \alpha} + \sum_{\langle i, j \rangle} \sum_{\alpha, \beta, \beta'} c_{i, \beta, \alpha}^\dagger V_{i, \beta, j, \beta'} c_{j, \beta', \alpha} \\ & + \lambda_{\text{ISO}}^p \mathbf{L} \cdot \boldsymbol{\sigma} + i \lambda_{\text{ISO}}^s \sum_{\langle\langle i, j \rangle\rangle} \sum_{\alpha} c_{i, s, \alpha}^\dagger \sigma_{\alpha\alpha}^z v_{ij} c_{j, s, \alpha} \\ & + i \sum_{\langle i, j \rangle} \sum_{\alpha, \beta, \beta'} c_{i, \beta, \alpha}^\dagger \gamma_{i, \beta, j, \beta'} [\hat{\mathbf{z}} \cdot (\boldsymbol{\sigma} \times \mathbf{r}_{ij})]_{\alpha\beta} c_{j, \beta', \beta}, \quad (1) \end{aligned}$$

where i, j represent lattice sites, $\langle i, j \rangle$ are nearest-neighbor sites (connecting vector \mathbf{r}_{ij}), α, β denote spin (\uparrow, \downarrow), and β, β' represent orbitals. The first term in Eq. (1) incorporates the on-site energies E_b , and the second term incorporates nearest-neighbor couplings $V_{i, \beta, j, \beta'}$. The third (on-site) term ($\propto \lambda_{\text{ISO}}^p$) is the intrinsic SOC in the p sector, \mathbf{L} being the orbital angular momentum and $\mathbf{S} = \boldsymbol{\sigma}/2$ the spin. The fourth term ($\propto \lambda_{\text{ISO}}^s$) encodes the intrinsic SOC in the s sector, with $\langle\langle i, j \rangle\rangle$ representing next-nearest-neighbor sites and $v_{ij} = \pm 1$, with the sign depending on the outer product of the two nearest-neighbor vectors that connect sites i and j [2]. The last term ($\propto \gamma_{i, \beta, j, \beta'}$) in the form of a nearest-neighbor hopping is the Rashba SOC.

This effective Hamiltonian can describe different types of 2D TIs on a honeycomb lattice [31,33], including Xenex [34]. Here, for reasons detailed below, we have chosen to consider a system that we have recently studied, namely a honeycomb superlattice formed by the attachment of HgTe nanocrystals [32]. The distance between nearest-neighbor sites, determined by the nanocrystal size, is 5 nm. Each nanocrystal can be seen as an artificial atom because its lowest empty states behave like s and p orbitals. Therefore, it was possible to describe the conduction-band structure of the HgTe superlattice using

*christophe.delerue@iemn.univ-lille1.fr

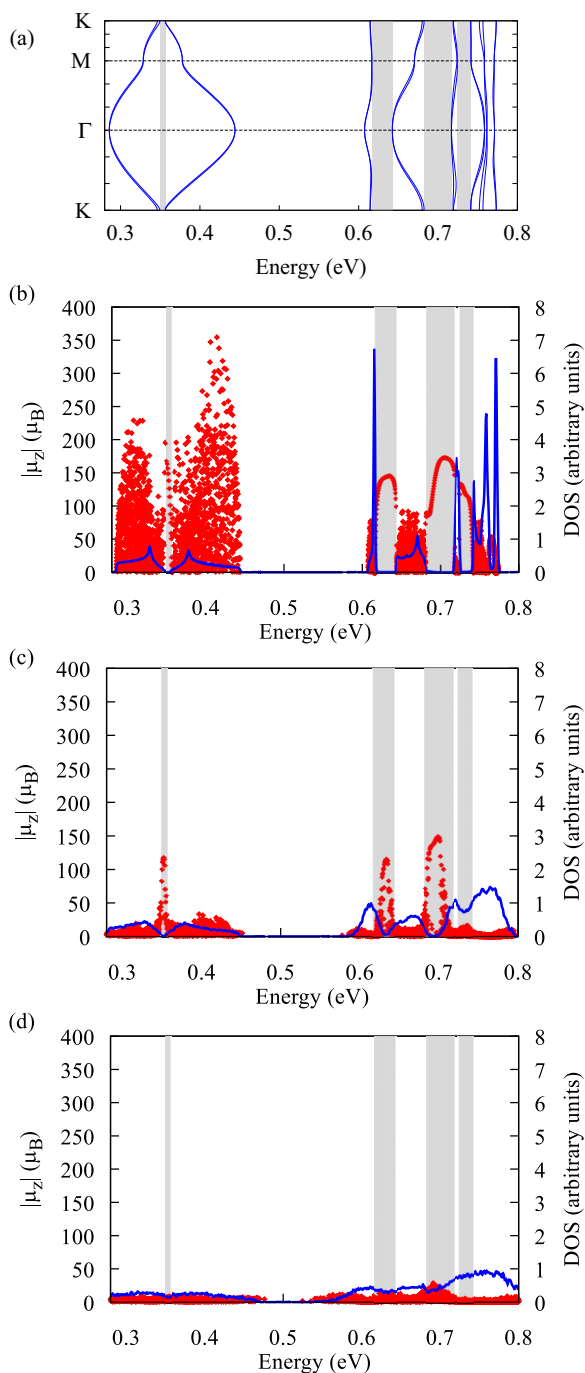


FIG. 1. (a) Bulk band structure of the multiorbital honeycomb lattice (inverted representation, \mathbf{k} vector along the vertical axis). The gray regions highlight the nontrivial topological gaps. (b)–(d) DOS (blue solid line) and MMs $|\mu_z|$ (red \blacksquare) vs the energy of each state for a TI-QD with a diameter of 300 nm. The results are obtained for different disorder strengths: $\sigma = 0$ meV (a), $\sigma = 15$ meV (b), and $\sigma = 35$ meV (c).

the effective Hamiltonian of Eq. (1). The corresponding Hamiltonian parameters are given in Ref. [32], and in the Supplemental Material [35].

Due to the combination of the multiorbital degrees of freedom [31,33] and the strong SOC, the band structure of the bulk lattice [Fig. 1(a)] exhibits several energy gaps. The

on-site energy for s orbitals (0.365 eV) being much smaller than for p orbitals (~ 0.7 eV), the manifolds of s and p bands are separated by a large trivial gap (0.45–0.61 eV). Four gaps, highlighted by gray regions in Fig. 1(a), have a nontrivial topological character ($\nu = 1$) [32]. In the following, these topological gaps will be denoted by E_{g_i} numbered in ascending order of energy ($i \in [1,4]$). The bands between 0.28 and 0.45 eV, mainly derived from s orbitals, have the same type of dispersion as the π bands in graphene [36], but they exhibit a small gap (E_{g_1}) at K due to the intrinsic SOC [2]. The bands between 0.61 and 0.78 eV come from p states. Some of them have a very flat dispersion, particularly due to the destructive interference of electron hopping induced by the honeycomb geometry [37]. The nontrivial gaps E_{g_i} in the p sector ($i \in [2,4]$) are very large due to the strong on-site SOC [32]. This system of rich topological properties is ideal to study the effect of topological protection against disorder on electronic states and MMs.

Starting from the honeycomb lattice, we built TI-QDs (flakes) of circular geometry. We checked that the effective Hamiltonian provides a very good description of their electronic structure and MMs compared to fully atomistic calculations performed on real systems made of nanocrystals (see the Supplemental Material [35]). The use of the effective Hamiltonian enables the study of large flakes, up to a diameter of 300 nm. A magnetic field perpendicular to the TI-QDs (z axis) is introduced using Peierls substitution [38]. The MM for a state of energy E is extracted from the splitting of the Kramers doublet as $\mu_z = -\partial E / \partial B$. The disorder is introduced as a random on-site potential with a Gaussian distribution of a standard deviation σ . Interestingly, this type of disorder mimics a real one reported recently in superlattices of self-assembled nanocrystals [39] (see the Supplemental Material [35]).

Figure 1(b) shows the density of states (DOS) and the MM of each state for the largest investigated TI-QD, in the absence of disorder. Peaks in the DOS appear at the positions of the quasiflat bands of the bulk lattice [Fig. 1(a)]. As expected [1–3], all states in nontrivial gaps have a wave function localized on the edge (see below). Large MMs arise in both types of states (up to $355\mu_B$ for band states and $173\mu_B$ for edge states). Edge-state MMs present bell curves versus energy inside each nontrivial gap (see the zoomed-in figures in the Supplemental Material [35]). On the contrary, band-state MMs form clouds of scattered values disregarding their energy.

The relative orientation of the spin momentum and the MM is analyzed via calculation, for each state, of the product $\mu_z \langle S_z \rangle$. Figure 2 shows that for edge states, $\mu_z \langle S_z \rangle$ is always

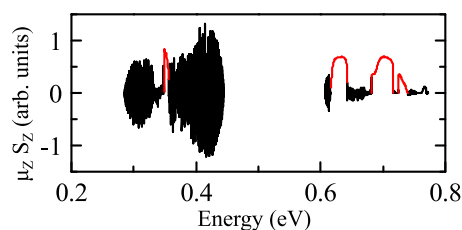


FIG. 2. Normalized product $\mu_z \langle S_z \rangle$ vs energy for each state of a TI-QD (diameter = 300 nm). A solid line links all the obtained points. The red lines highlight the results in nontrivial gaps.

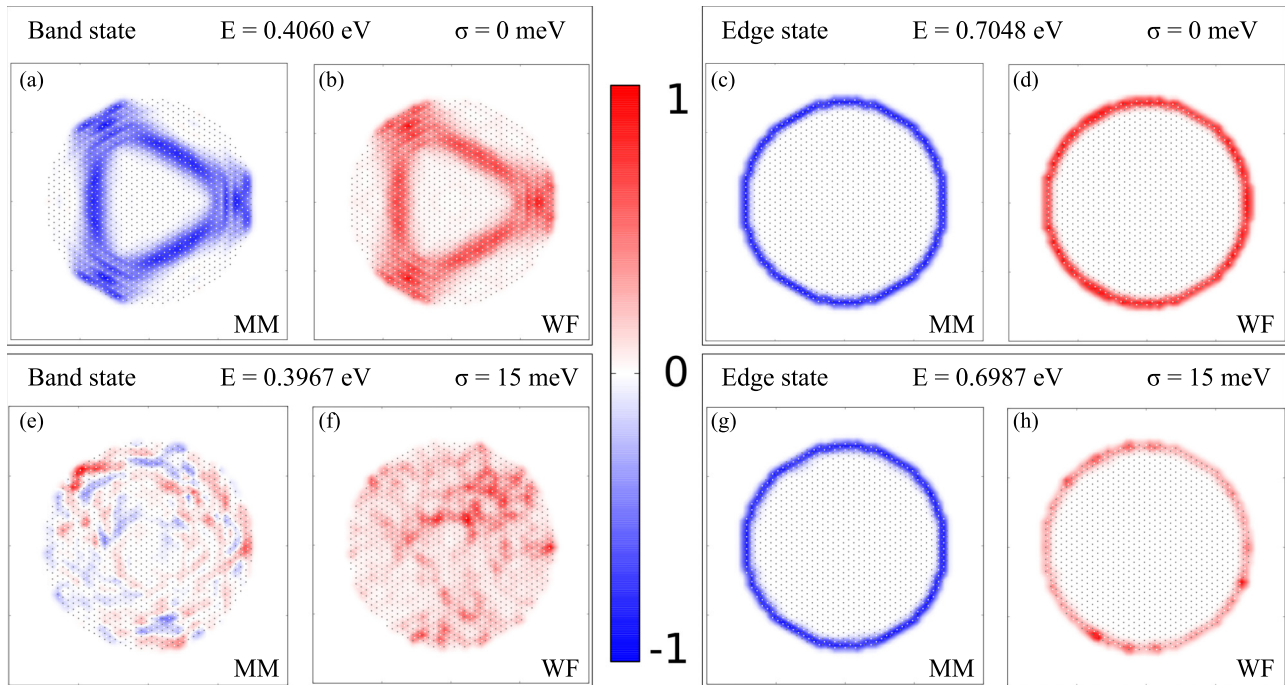


FIG. 3. Squared wave function (WF) [(b), (d), (f), and (h)] and magnetic moment (MM) [(a), (c), (e), and (g)] densities per site for band states [left panels: (a), (b), (e), and (f)] and edge states [right panels: (c), (d), (g), and (h)]. The upper panels [(a)–(d)] are calculated in the absence of disorder, while the lower panels [(e)–(h)] are obtained for $\sigma = 15$ meV. The energy of the states is indicated in each block.

positive, reflecting their helical character. For band states, the product can take both signs in a random manner.

The origin of the MMs in edge states can be understood with a semiclassical approach (see the Supplemental Material [35]). For a 1D ribbon, edge states form bands crossing the nontrivial gap in which electrons have momentum $\mathbf{p} = m_0 \hbar^{-1} \partial E / \partial \mathbf{k}$ locked to the spin [2]. In TI-QDs, for a given spin orientation, this leads to persistent current loops that generate orbital magnetization with angular momentum $\mathbf{L} = \mathbf{r} \times \mathbf{p}$. This also explains the bell curves, since \mathbf{p} is maximum somewhere near the center of the nontrivial gaps.

This simple description cannot be applied to band states. The origin of band-state MMs can be understood more generally in terms of SOICCs [40]. Whatever the electronic state, the SOC creates orbital motion leading to circulating currents determined locally by the spin-orbital components of the electron wave function. Figures 3(a) and 3(b) show the wave function and the density of the MM per site for a band state, while Figs. 3(c) and 3(d) show the wave function and the density of the MM per site for an edge state. The density of the MM reveals the existence of widely extended current loops for both states, at the origin of the large MMs [40].

SOICC loops are not intrinsically protected against disorder. Therefore, under moderate disorder, Fig. 1(c) shows a spectacular transition. All band-state MMs collapse while edge-state MMs remain nearly unchanged (maximum above $150\mu_B$). The DOS also shows that states with very small MMs appear in the nontrivial gap. These states start to enter from the band edges, hence reducing the nontrivial gap widths. At strong disorder, the nontrivial gaps are fully closed [Fig. 1(d)]. Then all MMs collapse, even for edge states.

In the presence of moderate disorder, the MM density of edge states is preserved [Fig. 3(g)] because the wave functions and therefore the current loops are topologically protected [Fig. 3(h)]. On the contrary, the localization of band-state wave functions induced by disorder [Fig. 3(f)] is responsible for the decrease of their MM [Fig. 3(e)]. Band-state SOICCs still exist, but the current loops become very small.

A detailed study for various TI-QD diameters D and disorder strengths σ is summarized in Fig. 4. For each value of σ , we average over ten disorder configurations. For the sake of comparison, we define the maximum MM in the bands ($\mu_{z,b}^>$), in the i th topological gap ($\mu_{z,g_i}^>$), and in all gaps ($\mu_{z,g}^>$). In any case, $\mu_{z,b}^>$ and $\mu_{z,g}^>$ follow a linear variation with D [Figs. 4(a) and 4(b)], the maximum diameter of the current loops increasing linearly with D . In the absence of disorder, the slopes of $\mu_{z,b}^>(D)$ and $\mu_{z,g}^>(D)$ have a comparable level. For weak disorder, this slope strongly decreases for band states, whereas it remains almost unaffected for edge states. This demonstrates the immediate and drastic effect of band-state localization on SOICCs.

For sufficiently strong disorder, the MM also collapses for edge states [Fig. 4(a)]. This defines a wide range of disorder strength, where edge states can be clearly identified through the measurement of their MM. However, Fig. 4(c) shows that the effect of the disorder is not identical in all topological gaps. In the p sector ($i \in [2, 4]$), a value of σ of the order of the energy gap E_{g_i} leads to a quasicomplete reduction of the edge-state MM, whereas in the s sector, a much higher value of σ/E_{g_1} is necessary to quench the MM at a similar level. This is also visible in Fig. 1(c), which shows that, for the same value of σ , the MMs remain much higher in the first gap than in the fourth

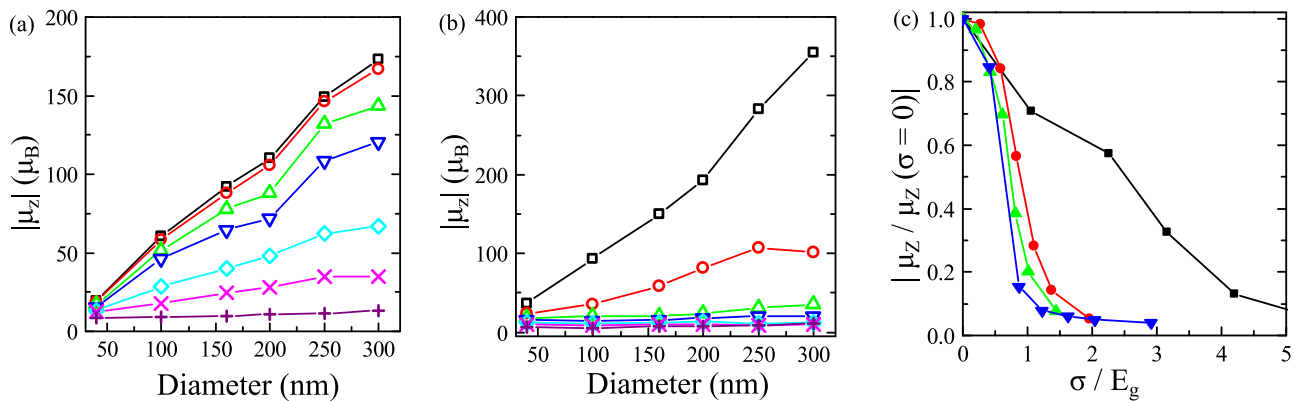


FIG. 4. Evolution of the maximum MM $\mu_{z,g}^>$ for edge states (a) and $\mu_{z,b}^>$ for band states (b) vs the TI-QD diameter D for different values of the disorder strength: $\sigma = 0$ meV (black \square), 7 meV (red \circ), 15 meV (green \triangle), 21 meV (blue ∇), 28 meV (cyan \diamond), 35 meV (magenta \times), and 50 meV (purple $+$). (c) Maximum MM $\mu_{z,g_i}^>$ for edge states in the first (black \blacksquare), second (red \bullet), third (green \blacktriangle), and fourth (blue \blacktriangledown) nontrivial gaps. In each case, $\mu_{z,g_i}^>$ is normalized with respect to its value at $\sigma = 0$ and is plotted vs σ / E_g^i , where E_g^i is the width of the i th topological gap ($D = 300$ nm).

one, even if E_{g_1} is smaller than E_{g_4} . This behavior results from the combination of two effects on the energy gap in the s sector: first its topological protection, and second its position at the K Dirac point at which the gap is opened by the SOC [2]. As a matter of fact, numerical simulations on graphene π bands have shown that moderate on-site disorder ($\sigma < V_{i,s;j,s}$) does not destroy the Dirac cone and its vanishing DOS at the Dirac point, rather it just leads to a renormalization of the group velocity [41–43]. This extra protection against disorder does not exist in the p sector, where the topological gaps are surrounded by regions with a high DOS. This is especially true in gaps in contact with quasiflat bands in which the disorder easily brings states from the bands to the gaps. This explains the fast decrease of the MMs in the fourth gap under increasing disorder [Fig. 1(c)].

A clear analogy can be made between the evolution of the MMs in Figs. 4(a) and 4(b) and the evolution of the Z_2 invariant versus disorder, as described, for example, in Refs. [44,45]. In the presence of disorder, the 2D TI goes progressively from a nontrivial insulating state with $\nu = 1$ to a zero-gap state with $\nu = 0$, ν being averaged over disorder. The decrease of the Z_2 invariant exhibits two distinct regimes: a slow one for

weak disorder and a sharp one for larger disorder [44,45]. The behavior of edge-state MMs is therefore a direct illustration of such a transition. This is particularly interesting since, unlike the Z_2 invariant, MMs can be measured experimentally.

In conclusion, we have shown that the MM of electronic states in TI-QDs can be used as a probe to study the topological transition from a nontrivial phase to a trivial one, under the effect of disorder. Moreover, the drastically different behavior of the MMs between band states and edge states can be used to find evidence of the quantum spin Hall phase itself. Adding a relatively small amount of disorder to samples rapidly collapses all band-state MMs. This provides us with a direct way to identify topological states, since edge-state MMs are preserved and can reach very high values (presently hundreds of μ_B). Our work also shows that the degree of protection of edge-state MMs depends on the nature of the topological gaps. The gaps that open in well-defined Dirac cones receive extra protection thanks to the vanishing DOS at the Dirac point.

This work was supported by the French National Research Agency (ANR) project “Dirac-III-V” ANR-16-CE24-0007-01.

-
- [1] C. L. Kane and E. J. Mele, *Phys. Rev. Lett.* **95**, 146802 (2005).
[2] C. L. Kane and E. J. Mele, *Phys. Rev. Lett.* **95**, 226801 (2005).
[3] B. A. Bernevig, T. L. Hughes, and S.-C. Zhang, *Science* **314**, 1757 (2006).
[4] M. König, S. Wiedmann, C. Brüne, A. Roth, H. Buhmann, L. W. Molenkamp, X.-L. Qi, and S.-C. Zhang, *Science* **318**, 766 (2007).
[5] R. Roy, *Phys. Rev. B* **79**, 195322 (2009).
[6] A. Bansil, H. Lin, and T. Das, *Rev. Mod. Phys.* **88**, 021004 (2016).
[7] K. Sun, W. V. Liu, A. Hemmerich, and S. Das Sarma, *Nat. Phys.* **8**, 67 (2011).
[8] X.-J. Liu, K. T. Law, and T. K. Ng, *Phys. Rev. Lett.* **112**, 086401 (2014).
[9] N. Goldman, J. C. Budich, and P. Zoller, *Nat. Phys.* **12**, 639 (2016).
[10] A. V. Nalitov, D. D. Solnyshkov, and G. Malpuech, *Phys. Rev. Lett.* **114**, 116401 (2015).
[11] T. Karzig, C.-E. Bardyn, N. H. Lindner, and G. Refael, *Phys. Rev. X* **5**, 031001 (2015).
[12] D. D. Solnyshkov, A. V. Nalitov, and G. Malpuech, *Phys. Rev. Lett.* **116**, 046402 (2016).
[13] Z. Yang, F. Gao, X. Shi, X. Lin, Z. Gao, Y. Chong, and B. Zhang, *Phys. Rev. Lett.* **114**, 114301 (2015).
[14] C. He, X. Ni, H. Ge, X.-C. Sun, Y.-B. Chen, M.-H. Lu, X.-P. Liu, and Y.-F. Chen, *Nat. Phys.* **12**, 1124 (2016).
[15] C. L. Kane and T. C. Lubensky, *Nat. Phys.* **10**, 39 (2013).
[16] R. Süssstrunk and S. D. Huber, *Science* **349**, 47 (2015).

- [17] A. Roth, C. Brüne, H. Buhmann, L. W. Molenkamp, J. Maciejko, X.-L. Qi, and S.-C. Zhang, *Science* **325**, 294 (2009).
- [18] C. Brune, A. Roth, H. Buhmann, E. M. Hankiewicz, L. W. Molenkamp, J. Maciejko, X.-L. Qi, and S.-C. Zhang, *Nat. Phys.* **8**, 485 (2012).
- [19] K. C. Nowack, E. M. Spanton, M. Baenninger, M. König, J. R. Kirtley, B. Kalisky, C. Ames, P. Leubner, C. Brüne, H. Buhmann, L. W. Molenkamp, D. Goldhaber-Gordon, and K. A. Moler, *Nat. Mater.* **12**, 787 (2013).
- [20] Y. Xia, D. Qian, D. Hsieh, L. Wray, A. Pal, H. Lin, A. Bansil, D. Grauer, Y. S. Hor, R. J. Cava, and M. Z. Hasan, *Nat. Phys.* **5**, 398 (2009).
- [21] Y. L. Chen, J. G. Analytis, J.-H. Chu, Z. K. Liu, S.-K. Mo, X. L. Qi, H. J. Zhang, D. H. Lu, X. Dai, Z. Fang, S. C. Zhang, I. R. Fisher, Z. Hussain, and Z.-X. Shen, *Science* **325**, 178 (2009).
- [22] D. Hsieh, Y. Xia, D. Qian, L. Wray, F. Meier, J. H. Dil, J. Osterwalder, L. Patthey, A. V. Fedorov, H. Lin, A. Bansil, D. Grauer, Y. S. Hor, R. J. Cava, and M. Z. Hasan, *Phys. Rev. Lett.* **103**, 146401 (2009).
- [23] L. Fu, C. L. Kane, and E. J. Mele, *Phys. Rev. Lett.* **98**, 106803 (2007).
- [24] L. Fu and C. L. Kane, *Phys. Rev. B* **76**, 045302 (2007).
- [25] J. E. Moore and L. Balents, *Phys. Rev. B* **75**, 121306 (2007).
- [26] Y. Oreg, G. Refael, and F. von Oppen, *Phys. Rev. Lett.* **105**, 177002 (2010).
- [27] R. M. Lutchyn, J. D. Sau, and S. Das Sarma, *Phys. Rev. Lett.* **105**, 077001 (2010).
- [28] X.-L. Qi and S.-C. Zhang, *Rev. Mod. Phys.* **83**, 1057 (2011).
- [29] K. Chang and W.-K. Lou, *Phys. Rev. Lett.* **106**, 206802 (2011).
- [30] P. Potasz and J. F.-Rossier, *Nano Lett.* **15**, 5799 (2015).
- [31] G.-F. Zhang, Y. Li, and C. Wu, *Phys. Rev. B* **90**, 075114 (2014).
- [32] W. Beugeling, E. Kalesaki, C. Delerue, Y.-M. Niquet, D. Vanmaekelbergh, and C. M. Smith, *Nat. Commun.* **6**, 6316 (2015).
- [33] J. W. F. Venderbos, M. Daghofer, and J. van den Brink, *Phys. Rev. Lett.* **107**, 116401 (2011).
- [34] A. Molle, J. Goldberger, M. Houssa, Y. Xu, S.-C. Zhang, and D. Akinwande, *Nat. Mater.* **16**, 163 (2017).
- [35] See Supplemental Material at <http://link.aps.org/supplemental/10.1103/PhysRevB.95.235426> for the corresponding Hamiltonian parameters, for zoomed-in views of Fig. 1, and for results of atomistic calculations.
- [36] A. H. C. Neto, F. Guinea, N. M. R. Peres, K. S. Novoselov, and A. K. Geim, *Rev. Mod. Phys.* **81**, 109 (2009).
- [37] C. Wu, D. Bergman, L. Balents, and S. Das Sarma, *Phys. Rev. Lett.* **99**, 070401 (2007).
- [38] M. Graf and P. Vogl, *Phys. Rev. B* **51**, 4940 (1995).
- [39] K. Whitham, J. Yang, B. H. Savitzky, L. F. Kourkoutis, F. Wise, and T. Hanrath, *Nat. Mater.* **15**, 557 (2016).
- [40] J. van Bree, A. Y. Silov, P. M. Koenraad, and M. E. Flatté, *Phys. Rev. Lett.* **112**, 187201 (2014).
- [41] B. Y.-K. Hu, E. H. Hwang, and S. Das Sarma, *Phys. Rev. B* **78**, 165411 (2008).
- [42] A. Lherbier, B. Biel, Y.-M. Niquet, and S. Roche, *Phys. Rev. Lett.* **100**, 036803 (2008).
- [43] M. Amini, S. A. Jafari, and F. Shahbazi, *Europhys. Lett.* **87**, 37002 (2009).
- [44] A. M. Essin and J. E. Moore, *Phys. Rev. B* **76**, 165307 (2007).
- [45] H.-H. Hung, A. Barr, E. Prodan, and G. A. Fiete, *Phys. Rev. B* **94**, 235132 (2016).